

Achieving Significant Multilevel Modulation in Superior-quality Organic Spin Valve

Cheng Zhang, Shuaishuai Ding,* Yuan Tian, Yunzhe Ke, Jian-Tao Wang, Jing Wang, Fengxia Hu,* Wenping Hu, and Baogen Shen*

Organic semiconductors, characterized by their exceptionally long spin relaxation times (\approx ms) and unique spinterface effects, are considered game-changers in spintronics. However, achieving high-performance and wide-range tunable magnetoresistance (MR) in organic spintronic devices remains challenging, severely limiting the development of organic spintronics. This work combines straintronic multiferroic heterostructures with organic spin valve (OSV) to develop a three-terminal OSV device with a gate structure. The device exhibits a record-high MR ratio of 281% which 10 times higher than the average in polymer systems. More importantly, this work can perform multilevel writing operations on the device using gate voltages and create at least 10 stable spin-dependent working states within a single device. Both experiments and theoretical calculations confirm such an extraordinary tunability range originates from the synergistic effects of strain and charge accumulation that amplified by the spinterface. This study demonstrates the potential of OSV systems for efficient spin manipulation and highlights the spinterface as an ideal platform for amplifying spin effects for next-generation spintronic devices.

information storage and logic devices.^[1,2] A key test-bed in this field is the spin valve (SV), which is typically comprised of two ferromagnetic (FM) metals decoupled by a non-magnetic (NM) interlayer.^[3] In this device, spin-polarized carriers are electrically injected into the NM interlayer through the FM/NM interface and then transported across it before spin relaxation occurs, until they are detected by the other FM electrode to form distinctive binary resistance states according to spin-dependent scatterings. Therefore, optimizing the injection and transport processes of spin-polarized current is crucial for enhancing the core performance, that is, magnetoresistance (MR, commonly represented by the difference between high and low resistance states) of the device.^[4,5] Organic semiconductors (OSCs) with unique advantages, such as low cost, flexibility,

1. Introduction

Spintronics, focusing on the control and manipulation of spin degree freedom of electrons, has significantly advanced modern

solution-processibility, and chemical tailorability are competing candidates for next-generation electronic devices.^[6] Particularly, their intrinsic weak spin-scattering mechanisms exhibit spin relaxation times that are several orders of magnitude longer

C. Zhang, B. Shen
 Ningbo Institute of Materials Technology & Engineering
 Chinese Academy of Sciences
 Ningbo, Zhejiang 315201, China
 E-mail: shenbg@iphy.ac.cn

C. Zhang, J.-T. Wang, J. Wang, F. Hu, B. Shen
 Beijing National Laboratory of Condensed Matter Physics & Institute of Physics
 Chinese Academy of Sciences
 Beijing 100190, China
 E-mail: fxhu@iphy.ac.cn

S. Ding, Y. Ke, W. Hu
 Key Laboratory of Organic Integrated Circuit
 Ministry of Education & Tianjin Key Laboratory of Molecular Optoelectronic Sciences
 Department of Chemistry
 Institute of Molecular Aggregation Science
 School of Science
 Tianjin University
 Tianjin 300072, China
 E-mail: dingshuaishuai@tju.edu.cn

Y. Tian
 School of Physics & Electronics
 Hunan University
 Hunan 410082, China
 J.-T. Wang, F. Hu, B. Shen
 School of Physical Sciences
 University of Chinese Academy of Sciences
 Beijing 100049, China

J.-T. Wang, F. Hu
 Songshan Lake Materials Laboratory
 Dongguan, Guangdong 523808, China

W. Hu
 Joint School of National University of Singapore and Tianjin University
 International Campus of Tianjin University
 Binhai New City, Fuzhou 350207, China

B. Shen
 Ganjiang Innovation Academy
 Chinese Academy of Sciences
 Ganzhou, Jiangxi 341000, China

 The ORCID identification number(s) for the author(s) of this article can be found under <https://doi.org/10.1002/adma.202416629>

DOI: 10.1002/adma.202416629

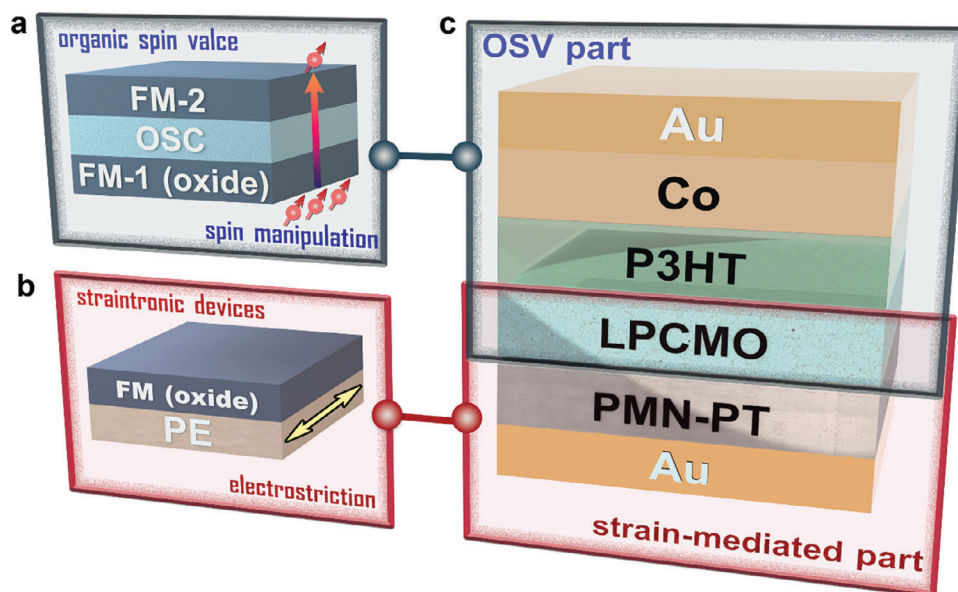


Figure 1. Conceptual diagram of the organic spin valve (OSV) device integrating strain control and spin-polarized current control. Basic structures and operating principles of a) the OSV device and b) the straintronic device, with FM representing the ferromagnetic layer, OSC representing the organic semiconductor layer, and PE representing the piezoelectric layer. c) The OSV device integrated with strain control and amplification effect from the spinterface. The blue area represents the OSV part, while the red area represents the strain-mediated part.

(\approx ms) than their inorganic counterparts (\approx ns), making them well-suited for the transport of spin signals.^[7–14] While half-metallic perovskite oxides, with \approx 100% spin polarization predicted and atomically smooth surfaces, are ideal candidates for enhancing interface effects and increasing the injection efficiency of spin-polarized currents.^[15,16] Notably, research on spinterface, a unique spin-dependent hybrid interfacial state that is only formed at the interface between the inorganic FM electrode and organic NM semiconductors, has offered versatility of spin injection not present in inorganic materials for the next-generation spintronic devices.^[17–20] Therefore, the organic spin valve (OSV) devices (Figure 1a) that combine the advantages of these two material types not only theoretically offer dual benefits in spin injection and transport but also establish a unique platform for the efficient regulation of devices through spin-related interface effects.

Turning the theoretical advantages of the innovative combination of organic and inorganic materials into reality to achieve high-performance OSV devices is the relentless pursuit of organic spintronics. Despite extensive efforts and breakthroughs in various aspects,^[21–38] the small MR signal (\approx 10%) and poor tunability (limited to binary states, R_{AP} and R_P) of OSV devices have continually hindered the realization of this goal.^[39] Although a few studies have reported that OSV devices can be modulated using indirect means such as pre-set magnetic fields or optical writing, the straightforward electric writing and magnetic reading technique,^[40–42] widely used in inorganic systems, still lacking thus far in OSV devices. This bottleneck has become one of the most significant obstacles in constructing high-performance spintronic devices, thereby hindering the development of organic spintronics both academically and practically.^[18] Voltage-induced piezoelectric strain effects are frequently employed in perovskite oxides to modulate the fundamental physical prop-

erties of materials (Figure 1b).^[43] This approach has proven effective for modulating strain-charge-orbital-spin coupling effects in strongly correlated systems.^[44] This voltage-based modulation method, which has never been used in OSVs, offers advantages such as low power consumption and excellent compatibility with the traditional semiconductor industry.^[45] Furthermore, it provides a novel approach for achieving multilevel modulation of OSV devices using straightforward electrical control. At this stage, achieving multilevel spin-based control of MR in high-performance devices and uncovering the underlying mechanisms have become urgent priorities for the organic spintronics and the broader spintronics communities.

In this study, we combined strain engineering with spinterface to achieve efficient modulation in high-performance organic strain/spintronic devices for the first time (Figure 1c). In the vertically stacked PMN-PT/(La_{2/3}Pr_{1/3})_{5/8}Ca_{3/8}MnO₃ (LPCMO)/Poly(3-hexylthiophene-2,5-diyl) (P3HT)/AlO_x/Co/Au OSV device, we observed an MR value as high as 281%, which is among the highest reported. More importantly, by utilizing PMN-PT as a piezoelectric gate material, we can achieve continuous and efficient multilevel modulation of the MR simply using an electric field, significantly enhancing the storage density and controllability of the OSV. The device exhibited a remarkably tunable MR magnitude, ranging from 39% to 281%, a level of tunability that is rarely achieved in similar types of devices. (Table S1, Supporting Information). Compared to pre-set magnetic or optical regulation, using an electric field as a modulation technique reduces power consumption and greatly enhances the device's operability. By employing the three-terminal design, which has never been used in OSV devices before, we separated the write unit from the read unit, avoiding the signal attenuation and device breakdown that can occur when a large voltage is directly applied across the device

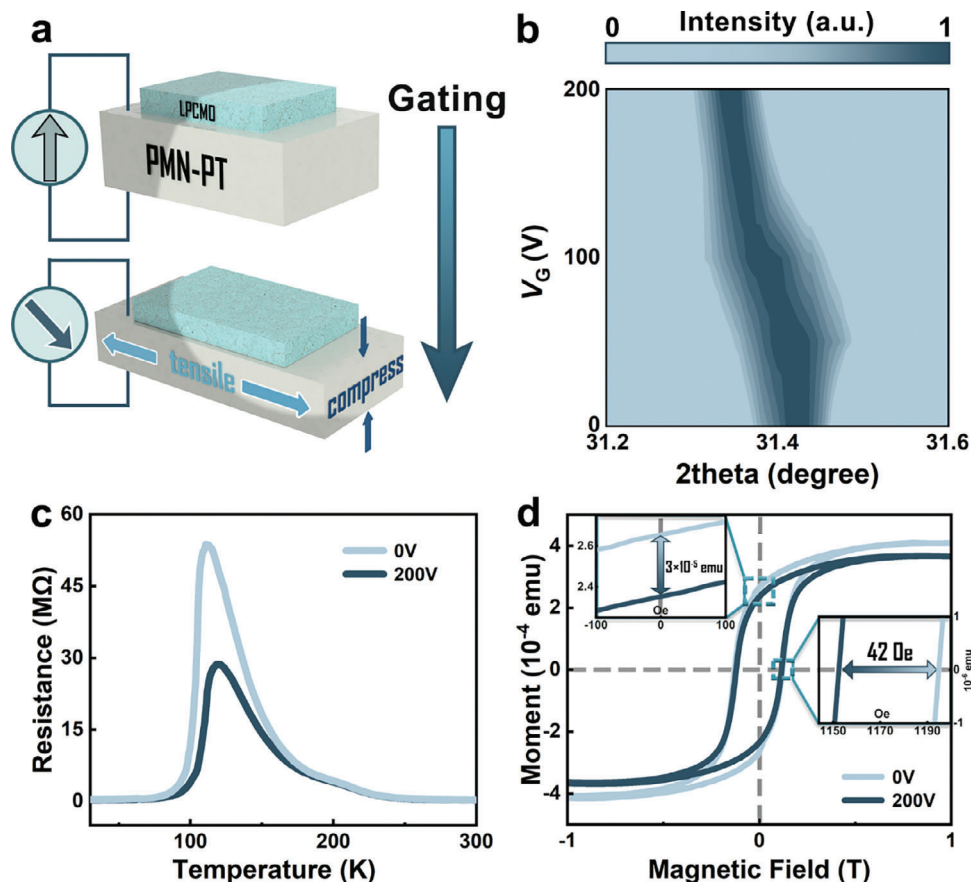


Figure 2. Control of magnet and electric properties of LPCMO by gate voltage via strain effect. a) Schematic of LPCMO/PMN-PT gate structure and the piezoresponse of PMN-PT under increased gate voltage. b) Evolution of the (011) diffraction peak of PMN-PT under in situ gate voltage application, with darker colors indicating higher diffraction peak intensity. c) The temperature dependence of resistance (R versus T) of the intrinsic LPCMO thin film under different gate voltages. d) The M - H curves of the LPCMO thin film under different gate voltages. The insets present the variations in remanent magnetization (M_r) and coercivity (H_c).

in traditional structures.^[1] Distinguished from the well-known straintronic mechanisms in inorganic systems, this efficient modulation is not solely achieved through strain-mediated coupling in ferromagnetic/piezoelectric structures.^[44–46] Instead, it relies more on the amplification effect of the spinterface on the interfacial magnetoelectric properties and potential changes, which can only be achieved in OSV devices. The integration of strain control and spin-polarized current control in OSVs allowed the realization of novel spin-based multi-resistance state modulation, for example, creating at least 10 stable working states within a single device, providing a unique strategy for integrated high-performance spintronic devices in the future.

2. Results and Discussion

2.1. Gate Voltage-Induced Strain Effect in PMN-PT/LPCMO

The piezoelectric single-crystal material $0.7[\text{Pb}(\text{Mg}_{1/3}\text{Nb}_{2/3})\text{O}_3] \cdot 0.3[\text{PbTiO}_3]$ (PMN-PT) can generate stable and controllable lattice strain under an applied electric field, making it an ideal choice for the gate material to control the FM oxide epitaxially grown

on top of it.^[47,48] Here we utilized the piezoelectric characteristics of PMN-PT to modulate the physical properties of FM electrodes LPCMO and therefore influence the subsequent spinterface in the whole devices. As shown in **Figure 2a**, under the electric field (the positive voltage is defined as the potential of PMN-PT relative to LPCMO while maintaining the LPCMO grounded), the PMN-PT (011) experiences compressive strain in the out-of-plane direction and tensile strain in the in-plane direction.^[49] This strain is subsequently transferred to the LPCMO thin film, which is epitaxially grown on top of the PMN-PT, thereby influencing the fundamental physical properties of the LPCMO. **Figure 2b** shows the evolution of (011) X-ray diffraction (XRD) peaks of PMN-PT under various gate voltages. As the gate voltage increases from 0 to 200 V, the peak position shifts noticeably toward a lower angle, indicating compression of the out-of-plane lattice and expansion of the in-plane lattice. Given that LPCMO is epitaxially grown on the PMN-PT substrate with high quality (Figure S1, Supporting Information), the LPCMO thin film undergoes strain-mediated magnetoelectric coupling as a result. This enables us to regulate the electrical (Figure 2c) and magnetic (Figure 2d) properties of LPCMO through the gate structure. Under a gate voltage of 200 V, the resistance of LPCMO

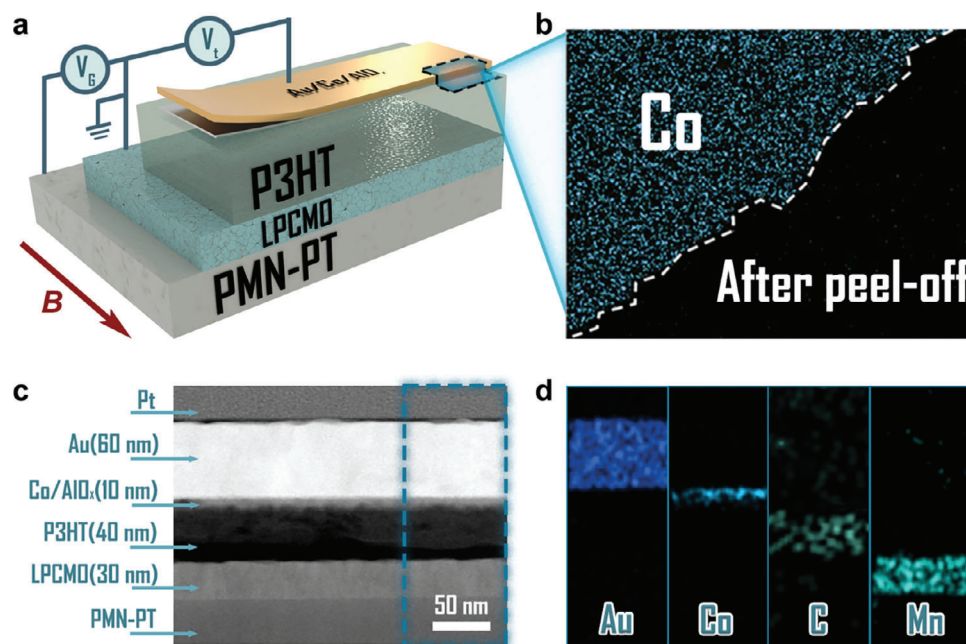


Figure 3. Structure and microscopy characterizations of the OSV device. a) The schematic diagram of the OSV device structure with vertical PMN-PT/LPCMO/P3HT/AIO_x/Co/Au configuration. The measurement voltage (V_t) is applied between the Au and LPCMO layers, while the gate voltage (V_G) is applied to the LPCMO and PMN-PT layers. During the test, the LPCMO layer is grounded to maintain zero potential. The external magnetic field B was applied in the plane. b) EDS mapping (Co element) of Co/P3HT interface. Part of the transferred Co electrode was removed using PDMS stamps to expose the boundary line between Co and P3HT. c) TEM cross-section images of the OSV prepared via the transfer technique and the corresponding d) EDS mapping results with characteristic elements for Au, Co, P3HT (C), and LPCMO (Mn) layers, respectively.

significantly decreases and the coercivity (H_C) of LPCMO decreases by 42 Oe, representing a 4% reduction compared to the H_C at 0 V. The change in the remanent magnetization (M_r) of LPCMO is even more pronounced, showing a 12% decrease (3×10^{-5} emu) compared to the original value. The detailed measurement methods are presented in Note S1 and Figure S2, Supporting Information. These changes in the fundamental magnetic and electrical properties of LPCMO under the gate voltage provide a crucial basis for the subsequent regulation of the device.

2.2. Reliable Gated-OSV with Damage-Free Spinterface

Building on the gate structure, we further constructed a vertically structured PMN-PT/LPCMO/P3HT/Co OSV device. As illustrated in Figure 3a, LPCMO and Co serve as the ferromagnetic electrodes, with a P3HT film as the spacer layer in between. The write (V_G) and read (V_t) terminals of the device are independently configured to prevent interference between the writing and reading processes. The bottom electrode, LPCMO, is a brand-new FM material that recently emerged in the field of OSVs. As a half-metal oxide, it exhibits very high spin polarization ($\approx 97\%$) and moderate conductivity compatible with organic materials, making it ideal for use as a spin injection layer to achieve efficient injection of spin-polarized currents.^[40,41] The semiconducting P3HT, a well-tested π -conjugated polymer commonly used in organic spintronic devices, was selected for its long spin relaxation time, commercial availability, and solu-

tion processability under ambient conditions. Additionally, its excellent film-forming properties result in a smoother surface (Figure S3a, Supporting Information), which facilitates the construction of high-quality interfaces. Our specially designed transferable method (see Experimental Section)^[27] was employed to avoid the common issue of metal penetration during the top electrode fabrication process.^[5,39] Additionally, a ≈ 1 nm semi-oxidized AIO_x layer was inserted at the FM/OSC interface to physically isolate P3HT from the chemically active Co. Figure 3b presents the energy-dispersive X-ray spectroscopy (EDS) image of as-transferred Co electrodes on P3HT interface, where the artificially exposed P3HT area without Co residual confirms the damage-free physical contact at the top spinterface. The scanning electron microscopy (SEM) micrograph of the corresponding peeled-off area is provided in Figure S4, Supporting Information. Figure 3c exhibits the overall cross-sectional transmission electron microscopy (TEM) image of our device, revealing sharp and smooth interfaces. From this image, we can determine the precise thickness of each layer in our device: LPCMO (30 nm), P3HT (40 nm), and Co (10 nm), which are consistent with those obtained from X-ray reflectometry (XRR) (Figure S5, Supporting Information) and atomic force microscopy (AFM) (Figure S3b, Supporting Information). Furthermore, corresponding EDS mapping indicates no element diffusion between different layers within the detection limits, demonstrating that our interface-engineered strategy effectively prevents intermixing and metal permeation (Figure 3d). The long-range homogeneous layers and sharp interfaces are essential for obtaining reliable and stable MR signals.

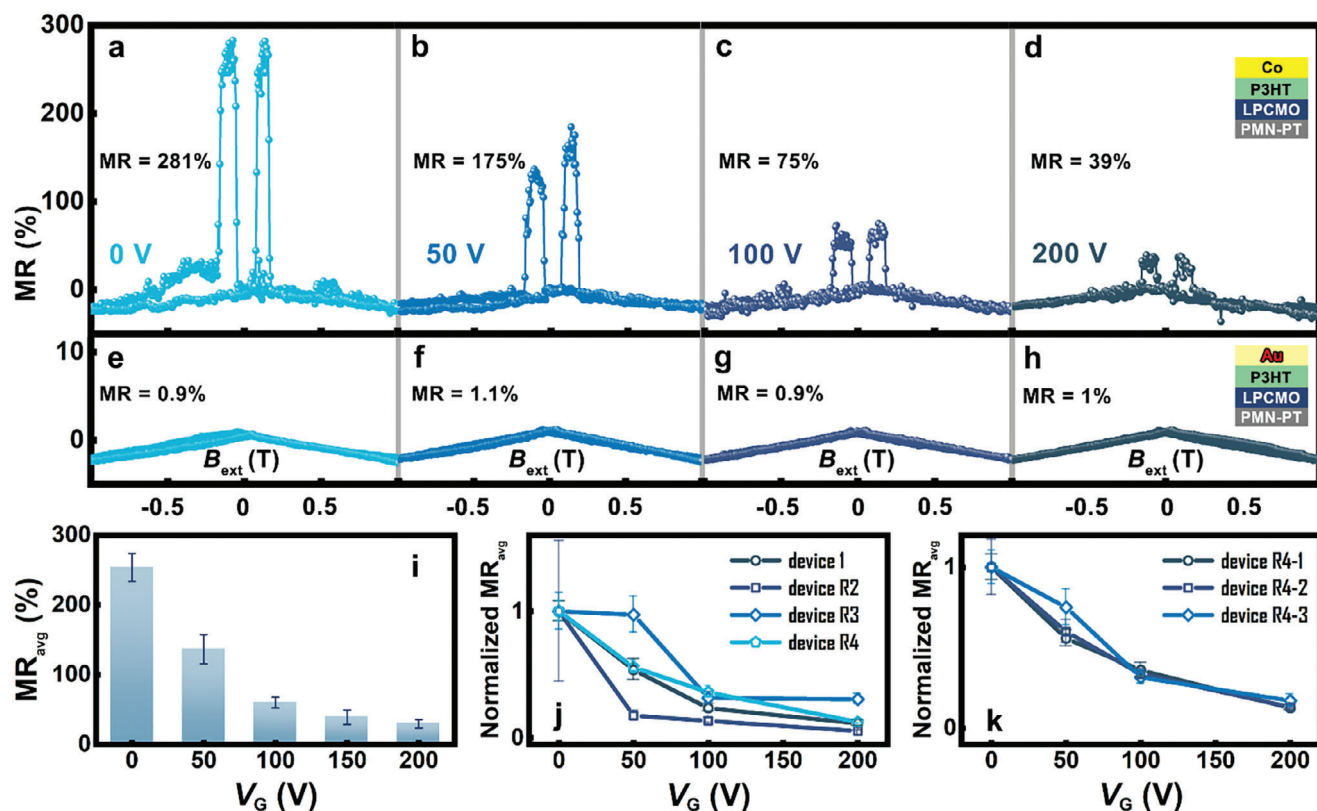


Figure 4. The spin-related MR modulation of the OSV. a–d) The MR responses of LPCMO/P3HT/Co OSV (Device 1) with different gate voltages. e–h) The MR responses of reference LPCMO/P3HT/Au (Device 2) with different gate voltages. The insets represent the device structures. All MR measurements were performed at $T = 30$ K using $V_t = 0.1$ V. i) The MR_{avg} values of LPCMO/P3HT/Co (device 1) under different V_G . The normalized MR_{avg} versus V_G curves of j) all four identical devices and k) device R4 from three repeatable testing procedures.

2.3. Multilevel MR Modulation in Gated-OSV Device

Figure 4a–d presents the MR curves of the OSV device (Device 1) as a function of V_G measured at 30 K using 0.1 V V_t . During the measurements, V_G was consistently applied across the gate, and the magnetic field was applied in the in-plane direction. The relative magnetization orientations of the two FM layers transition from parallel (P) to antiparallel (AP) and back to parallel (P) as the magnetic field sweeps from 1 T to -1 T and then returns to 1 T. The MR ratio is calculated as $MR = (R_{AP} - R_p)/R_p$, where R_{AP} and R_p represent the resistances of the OSV in the antiparallel and parallel magnetization configuration of the two FM electrodes, respectively. All MR curves exhibited positive MR ($R_p < R_{AP}$), and the resistance transition points corresponded well with the H_C of the LPCMO and Co electrodes in both trace and retrace field sweeps (Figure S6, Supporting Information). The abrupt changes with rapid responses between the parallel and antiparallel configuration confirm the well-defined interfaces in our device. The initial state (Figure 4a, $V_G = 0$ V) of the device exhibits a maximal MR signal close to +281%, which has reached the highest MR ratios ever reported in polymer spin valves (Figure S7, Supporting Information). The significant signal is primarily a result of our systematic optimization of the device: 1) The combination of organic and inorganic materials provides dual advantages in both injection and transport; 2) The undamaged FM/NM interface prevents spin scattering at the interface, increasing the ef-

fective spin diffusion length of the material; 3) The separation of the read and write units avoids performance degradation caused by high voltage. More importantly, the MR of the device can be distinctly modulated in multiple levels by the gate voltages. It is worth noting common OSVs with a basic sandwich structure and single working mechanism can only exhibit binary states of R_{AP} and R_p , making it challenging to achieve in situ continuous multilevel control. And unlike three-terminal devices such as organic field-effect transistors (OFETs) that manipulating current,^[50] we can effectively manipulate the spin state through the gate structure. As a demonstration, we applied four different gate voltages at the write terminal, thereby creating multiple stable operating states within a single device. All working states exhibited very sharp vertical resistance switches, which is challenging to achieve in most OSVs. As the gate voltage increases, the MR value of the device decreases monotonically. Under a gate voltage of 200 V, the MR value drops from 281% to 39%, which is still far above the average MR in polymer spin valve systems. This efficient MR modulation also establishes a new record for the tunable MR range in similar types of devices (Figure S7, Table S1, Supporting Information). To confirm that the MR signal modulation originates from spin state, we constructed a reference device without the second FM electrode of Co for spin detection, PMN-PT/LPCMO/P3HT/Au (Device 2), and tested its MR under the same conditions, as shown in Figure 4e–h. In this device, the original top magnetic electrode Co was replaced with a

non-magnetic electrode Au, thereby eliminating the resistive change caused by spin-dependent scattering. Without spin-polarized carriers, the MR value of Device 2 decreased from 281% to 0.9% and remained nearly constant under different gate voltages. These results demonstrate that the large MR signal and multilevel tunability observed in the OSV device are indeed due to spin transport and are unrelated to crosstalk signals such as anisotropic magnetoresistance (AMR) and tunneling anisotropic magnetoresistance (TAMR). Meanwhile, we fabricated three additional control devices (device R2, device R3, device R4) using the same process and tested them under identical conditions to verify reproducibility across different batches and multiple tests of a single device. The results are presented in Figure 4i–k. The consistent responses confirmed the reliability of our experimental results. The calculation method for MR, the statistical errors, and the additional MR data are provided in Note S2 and Figures S8–S10, Supporting Information.

2.4. Origins of Tunable MR States

To elucidate the necessary conditions for achieving a significant modulation in MR through gate control, it is essential to identify and analyze the key factors that influence this phenomenon. Here we designed two sets of comparative experiments, as shown in Figure 5. First, we need to determine whether the modulation effect of the device originates from the piezoelectric strain effect of PMN-PT. Although we demonstrated in Figures 2 and 4 that the gate voltage can simultaneously alter the fundamental physical properties of LPCMO and the MR value of the OSV device, we have not yet established a direct link between these two phenomena. To address this question, we designed a comparative device of SrTiO₃ (STO)/LPCMO/P3HT/Co (Device 3). In this device, the piezoelectric substrate PMN-PT was replaced with a standard substrate STO, which does not exhibit the piezoelectric strain effect. Consequently, applying a gate voltage to this device would not induce any strain effect. As shown in Figure 5a, the MR value of the device decreases monotonically with increasing gate voltage. Compared to Device 1, which exhibits a strain effect, both the absolute and relative changes in MR are significantly reduced (Figure 5a inset). This result highlights the crucial role of the strain effect in the modulation process of the OSV device. It is important to note that although the changes in Device 3 are small, they are not negligible. We will address this phenomenon in section 2.5. The second point to discuss is whether this modulation effect necessarily relies on the spinterface effect, that is, whether organic systems are indispensable for achieving efficient modulation. To address this, we constructed a comparative device, PMN-PT/LPCMO/Al₂O₃/Co (Device 4). In this device, the organic semiconductor P3HT was replaced with the inorganic material Al₂O₃. Since the spinterface effect only occurs at organic/inorganic hybrid interfaces, Device 4 lacks the spinterface effect presented in Device 1. As shown in Figure 5b, both the MR ratio and modulation amplitude of Device 4 are significantly reduced compared to Device 1, in which shows almost no change under varying gate voltages. This demonstrates the irreplaceable role of the spinterface effect in enhancing MR signal and achieving efficient modulation. So far, we can draw two

preliminary conclusions: 1) The stress effect induced by the gate voltage can effectively modulate the MR of the device; 2) Efficient modulation can only be achieved through the organic/inorganic hybrid spinterface.

2.5. Modulation Mechanisms and Amplification Effects of the Spinterface

The last unresolved issue is to illustrate why such a wide range of modulation can be achieved only in gated OSV systems. Considering the fact that even in Device 3 lacks a strain effect, we can still observe changes in the MR ratio, we believe the modulation is related to surface potential effects. Kelvin probe force microscopy (KPFM) was utilized to measure the surface potential. As shown in Figure 6a, the P3HT surface exhibited a higher electrochemical potential than the LPCMO film. And this potential difference between P3HT and LPCMO can be further amplified by applying gate voltages, as illustrated in Figure 6b. Since this charge accumulation effect occurs only in the interfacial region over a few nanometers, much smaller than the overall device scale, it typically does not impact inorganic systems.^[45,46] However, in OSV devices, spin-dependent energy level shifts and broadening occur at the van der Waals interfaces between the FM and OSC layers, known as the spinterface effect. This effect will significantly affect the effective spin polarization and only occurs in two to three molecular layers (≈ 2 nm) at the interface.^[18,51] Consequently, the accumulation of surface charges can greatly impact the spinterface effect, thereby affecting the spin injection and transport of the device. This explains why the MR signal of Device 3, which lacks the strain effect, can still be modulated by the electric field: although the STO substrate does not exhibit a piezoelectric strain effect, its relatively high intrinsic dielectric constant can lead to interfacial charge accumulation under gate voltages,^[52,53] thus influencing the device's performance, as shown in Figure 5a. Based on the above analysis, we conclude that there are two synergetic modulation mechanisms in the gate-structured PMN-PT/LPCMO/P3HT/Co OSV device: 1) strain-mediated magnetoelectric coupling and 2) interfacial potential effects due to charge accumulation, as illustrated in Figure 6c. These mechanisms are amplified by the spinterface effect, thereby regulating the overall device performance. This mechanism can be further supported by density functional theory (DFT) calculations, as demonstrated by the spin-resolved density of states (DOS) at the P3HT/LPCMO interface (Figure 6d). Both strain and interfacial potential influence the spin polarization (p) around the Fermi level. Specifically, under ① 0.5% compressive strain, ② a 100 mV interfacial potential, and ③+② their combined effect, the effective p at the spinterface decreases from the initial 54% to 45%, 33%, and 27%, respectively, exhibiting the same trend as the experimentally observed MR behavior. Hence, the tunability of the device indeed arises from the controllable spin injection process, which is associated with the variations in DOS at the spinterface. Detailed interfacial spin-resolved DOS information and calculation methods were provided in Figure S11 and Note S3, Supporting Information. For inorganic devices without the spinterface (Device 4), the impact of stress effects and charge accumulation under a 200 V gate voltage is minimal, making it difficult to modulate the MR values. In contrast, for OSV devices with the spinterface

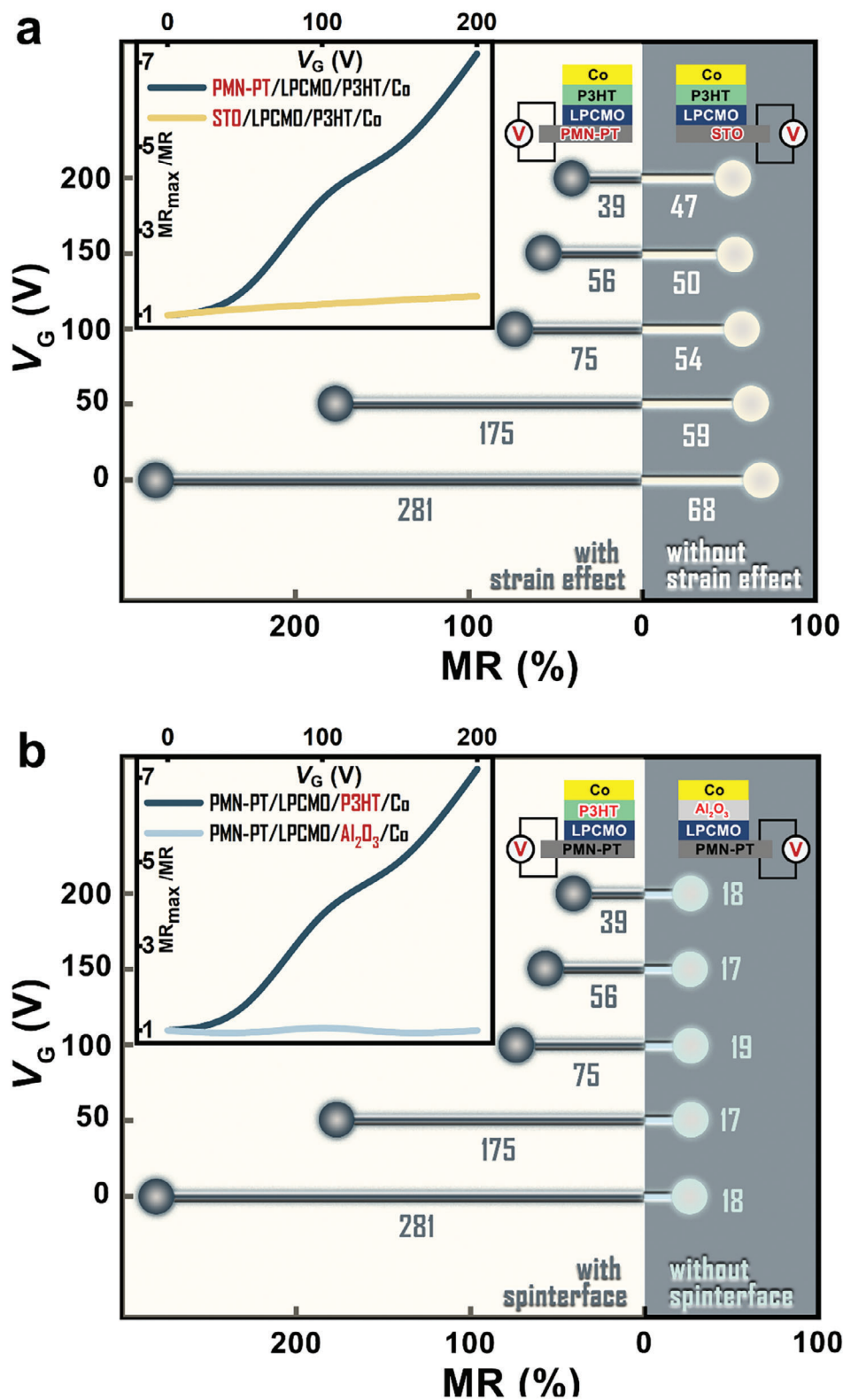


Figure 5. Key factors for achieving efficient MR modulation. a) Comparison of MR values under different gate voltages (V_G) in devices with strain effect (PMN-PT/LPCMO/P3HT/Co, left side of the figure) and without strain effect (STO/LPCMO/P3HT/Co, right side of the figure). b) Comparison of MR values under different (V_G) in devices with spinterface (PMN-PT/LPCMO/P3HT/Co, left side of the figure) and without spinterface (STO/LPCMO/P3HT/Co, right side of the figure). The inset shows calculated MR_{max}/MR as a function of V_G , representing the magnitude of MR variation under V_G modulation and the tunability of the device.

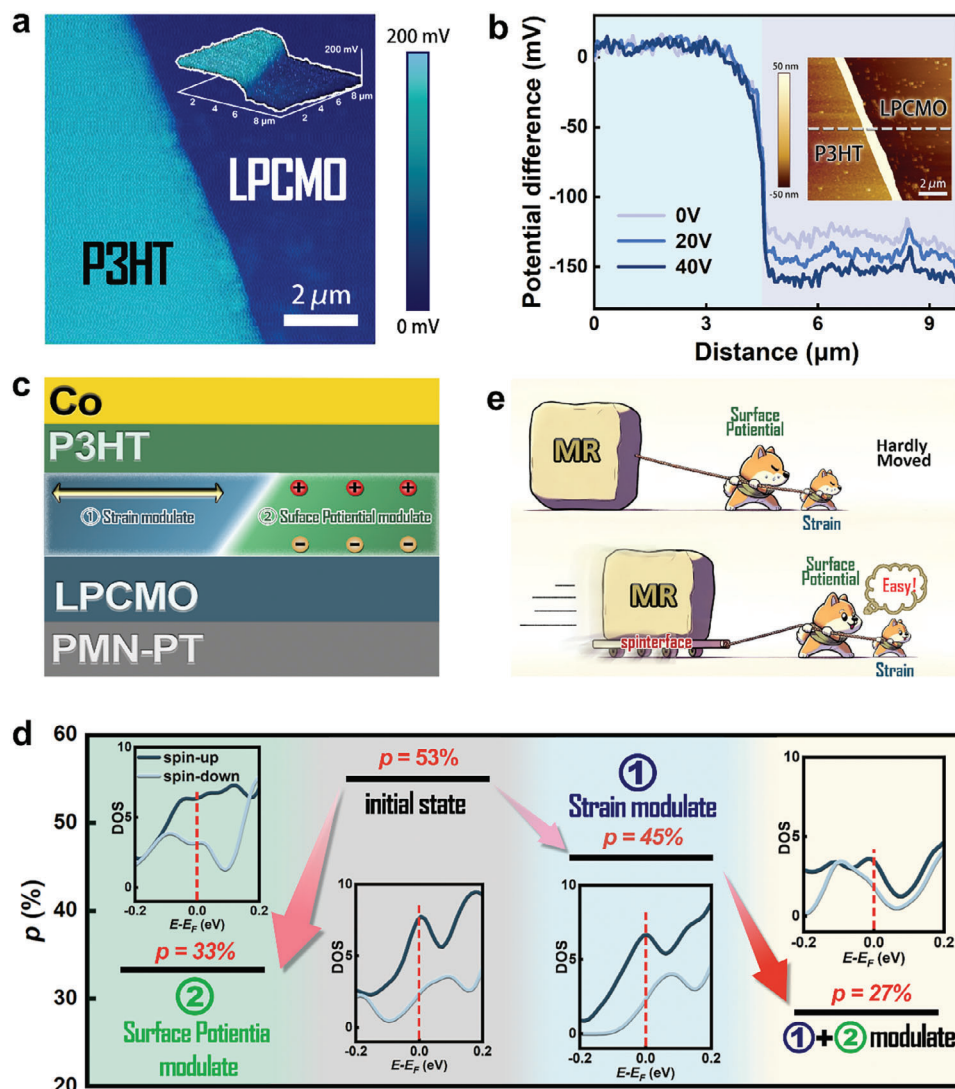


Figure 6. DFT calculations and the phenomenological model of spin-injection modulation at the spinterface. a) KPFM images of the P3HT/LPCMO heterostructure. P3HT was spin-coated entirely over LPCMO, and the left half of the P3HT was removed to expose the LPCMO surface. The inset shows the 3D version of the KPFM spectrum. b) Potential-difference profiling across the P3HT/LPCMO surface under different voltages. The inset images show the AFM topography for the corresponding area. c) Two modulation mechanisms of strain effect and surface potential effect acting on the spinterface. d) The calculated effective spin polarization (p) at the LPCMO/P3HT interface in the initial state, under ① 0.5% compressive stress, under ② a 100 mV interfacial potential, and under ①+② the combined influence of both factors. The inset shows the corresponding spin-resolved density of states (DOS) of the LPCMO/P3HT structures. e) Schematic illustration of enhancing device tunability using the spinterface.

(Device 1), the spinterface acts as leverage, significantly reducing the difficulty of MR modulation via stress effects and charge accumulation (Figure 6e). This “MR-leverage” effect enables the OSV devices to achieve large-scale multi-state modulation and storage functions that are challenging for traditional inorganic devices. With the help of the spinterface effect, we can efficiently control the operating spin-related states of the device, creating multiple stable working states within a single device (Note S4, Figure S12, Supporting Information). This demonstrates the potential of the OSV device for high-density, low-energy information storage applications, providing a new approach for the spin related control of OSV devices (Table S2, Supporting Information).

3. Conclusion

We have fabricated the first PMN-PT/LPCMO/P3HT/Co OSV with a gate structure, achieving a MR value of 281%, which is one of the highest MR values has been reported. More importantly, the spin-related working states of the device can be multi-level modulated using gate voltage, a capability not previously realized in OSVs. The MR value can be in situ modulated from 281% to 39%, setting a new record for the tunable MR range in similar devices. Further experimental results and DFT calculations confirm that the regulation of MR is driven by the synergistic effects of strain and charge accumulation, which are subsequently amplified through the spinterface. These findings highlight the

significant potential of OSVs for information storage and processing and expand the diversity of multifunctional spintronic devices. In the future, the electrically controlled spinterface effects in OSV devices warrant further exploration. This research promises to uncover new physical phenomena and functionalities, paving the way for the development of high-performance, low-energy, high-density next-generation electrically controlled integrated devices.

4. Experimental Section

Sample Preparation: The 30 nm $(\text{La}_{2/3}\text{Pr}_{1/3})_{5/8}\text{Ca}_{3/8}\text{MnO}_3$ (LPCMO) films were deposited on the $0.7[\text{Pb}(\text{Mg}_{1/3}\text{Nb}_{2/3})\text{O}_3]-0.3[\text{PbTiO}_3]$ (PMN-PT) substrate using a shadow mask with the pulsed laser deposition (PLD) technique. Before deposition, the PMN-PT is ultrasonically cleaned in ethanol for 15 min to clean its surface. During the deposition process, the O_2 pressure was maintained at 120 Pa, and the substrate temperature was held at 705 °C. The LPCMO/PMN-PT heterostructure were cooled to room temperature at a rate of 12 °C/min in an O_2 atmosphere of 2×10^4 Pa after the deposition process. Regioregular poly(3-hexylthiophene) (RR-P3HT, purchased from TCI Chemicals and used as received) was dissolved in *o*-dichlorobenzene (*o*-DCB) and was filtered through an organic phase syringe filter to form a solution with a concentration of 10 mg mL⁻¹. For the organic layer fabrication, uniform polymer film with a thickness of 40 nm was spin-coated onto the LPCMO/PMN-PT substrate at a rotation speed of 2000 rpm and was subsequently baked at 150 °C for 5 min in an ambient atmosphere to remove any residual solvents. To avoid the uncontrollable metal filaments that often caused by traditional thermal deposition methods, this work employed the PDMS-assisted mechanical transfer technique to fabricate the top FM electrodes.^[27] Specifically, a composite of ≈ 1 nm $\text{AlO}_x/10$ nm Co/60 nm Au metal was deposited on a silicon oxide substrate with poly(sodium 4-styrenesulfonate) (PSS, purchased from Sigma-Aldrich) sacrificial layer. The Al layer, with manageable oxidation to form AlO_x , was deposited by thermal evaporation at a rate of 0.1 \AA s^{-1} . Subsequently, the Co and Au layers were deposited by e-beam evaporation at rates of 0.1 and 0.5 \AA s^{-1} , respectively. A supporting layer of polystyrene (PS, purchased from Sigma-Aldrich) was then spin-coated on to the composite metal layers to form a self-encapsulated structure of PSS/ AlO_x /Co/Au/PSS. Next, the entire self-encapsulated structure was carefully exfoliated and carefully laminated onto the spin-coated P3HT spacing layer using the polydimethylsiloxane (PDMS Sylgard 184, purchased from Dow Corning Corporation) transfer stamp. The effective device area of the OSV device with a structure of PMN-PT/LPCMO/P3HT/ AlO_x /Co/Au/PSS, determined by two crossed FM electrodes, was $1 \text{ mm} \times 2 \text{ mm}$. For the control experiment, all preparation processes were exactly the same as those described above, with the corresponding steps omitted (Note S5, Table S3, Supporting Information). The fabrication process for all the devices was conducted in a cleanroom to avoid extra contamination.

Characterization and Measurement: The crystal structure of the oxides was measured using a Bruker X-ray reflectometry (XRR) and X-ray diffractometer (XRD) equipped with thin-film accessories (D8 Discover, Cu $K\alpha$ radiation). The thickness and surface morphology were determined using the atomic force microscope (AFM, Bruker Dimension Icon, tapping mode), and the surface potential was mapped in the KPFM mode. Scanning electron microscopy (SEM) images and corresponding energy-dispersive X-ray spectroscopy (EDS) mappings were collected using a Hitachi SU8010 SEM-EDS. The overall cross-sectional transmission electron microscopy (TEM) image and corresponding EDS mappings were measured using a FEI-Talos F200s TEM. The electrical transport measurements were conducted using a Physical Property Measurement System (PPMS Dynacool, Quantum Design) combined with Keithley 6517B High Resistance Meter and Keithley 2636B Dual-Channel System Source Meter Unit (SMU). All magnetic characteristics were measured using a superconducting quantum interference device (SQUID, Quantum Design). De-

tailed MR measurement protocols are provided in Figure S13, Note S5, Supporting Information.

Computational Methods: This density functional theory (DFT) calculations were performed using the Vienna ab initio simulation package (VASP) with the all-electron projector augmented wave method.^[54,55] The generalized gradient approximation in the Perdew–Burke–Ernzerhof (GGA-PBE) formulation^[56] was adopted with an energy cutoff of 500 eV. A supercell including two units of LPCMO and one monolayer of P3HT molecules was used to simulate the heterostructure. DFT-D3 method with Becke–Johnson damping function was adopted for the vdW-dispersion energy-correction to relax the LPCMO/P3HT interface.^[57] The spin polarization calculations with ferromagnetic state were carried with valence states $6s^2 5s^2 5p^6 5d^1$ for La, $4s^1 3d^6$ for Mn, $2s^2 2p^2$ for C, $2s^2 2p^4$ for O, $3s^2 3p^4$ for S, and $1s^1$ for H. Throughout this work, the Hubbard $U = 3$ eV was used to treat the localized 3d electrons of Mn in the GGA + U scheme.^[58] Convergence criteria employed for both the electronic self-consistent relaxation and the ionic relaxation are set to 10^{-6} eV and 0.01 eV \AA^{-1} for energy and force, respectively. In addition, an external electrostatic field of 5 mV \AA^{-1} is applied perpendicular to interface to simulate to the field effect. The electronic density of states (DOSs) are calculated with a denser point of 4000 (NEDOS = 4000).

Supporting Information

Supporting Information is available from the Wiley Online Library or from the author.

Acknowledgements

This work was supported by the Science Center of the National Science Foundation of China (52088101), the National Key Research and Development Program of China (2020YFA0711502, 2023YFA1406003, 2021YFA1400300, 2019YFA0704900, 2022YFB3603800), the National Natural Sciences Foundation of China (12404226, 52373250, 52003190, 62101185, 12374020, 92263202, U23A20550, 22361132534), the Strategic Priority Research Program (B, XDB33030200) and the Key Program of the Chinese Academy of Sciences (CAS). The authors thank the Haihe Laboratory of Sustainable Chemical Transformations for financial support.

Conflict of Interest

The authors declare no conflict of interest.

Data Availability Statement

The data that support the findings of this study are available from the corresponding author upon reasonable request.

Keywords

magnetoresistance, molecular spintronics, organic spin valves, quantum device, spin modulation

Received: October 30, 2024
Published online: November 26, 2024

[1] C. Chappert, A. Fert, F. N. Van Dau, *Nat. Mater.* **2007**, *6*, 813.

[2] V. A. Dediú, L. E. Hueso, I. Bergenti, C. Taliani, *Nat. Mater.* **2009**, *8*, 707.

- [3] I. Žutić, J. Fabian, S. D. Sarma, *Rev. Mod. Phys.* **2004**, *76*, 323.
- [4] L. Guo, X. Gu, X. Zhu, X. Sun, *Adv. Mater.* **2019**, *31*, 1805355.
- [5] S. Ding, Y. Tian, W. Hu, *Nano Res.* **2021**, *14*, 3653.
- [6] Y. Chen, L. Chen, B. Geng, F. Chen, Y. Yuan, D. Li, Y.-X. Wang, W. Jia, W. Hu, *SmartMat.* **2024**, *5*, e1229.
- [7] C. Barraud, P. Seneor, R. Mattana, S. Fusil, K. Bouzehouane, C. Deranlot, P. Graziosi, L. Hueso, I. Bergenti, V. Dediu, F. Petroff, A. Fert, *Nat. Phys.* **2010**, *6*, 615.
- [8] D. Li, G. Yu, *Adv. Funct. Mater.* **2021**, *31*, 2100550.
- [9] M. Wei, X. Lu, J. Qiao, S. Ren, X.-T. Hao, W. Qin, *ACS Nano* **2022**, *6*, 13049.
- [10] X. Liu, H. Li, W. Zhang, Z. Yang, D. Li, M. Liu, K. Jin, L. Wang, G. Yu, *Angew. Chem., Int. Ed.* **2023**, *62*, 202308921.
- [11] Z. Ni, H. Wang, H. Dong, Y. Dang, Q. Zhao, X. Zhang, W. Hu, *Nat. Chem.* **2019**, *11*, 271.
- [12] S. Duan, X. Gao, Y. Wang, F. Yang, M. Chen, X. Zhang, X. Ren, W. Hu, *Adv. Mater.* **2019**, *31*, 1807975.
- [13] Y. Gao, Y. Ke, T. Wang, Y. Shi, C. Wang, S. Ding, Y. Wang, Y. Deng, W. Hu, Y. Geng, *Angew. Chem., Int. Ed.* **2024**, *63*, 202402642.
- [14] L. Yuan, Y. Huang, X. Chen, Y. Gao, X. Ma, Z. Wang, Y. Hu, J. He, C. Han, J. Li, Z. Li, X. Weng, R. Huang, Y. Cui, L. Li, W. Hu, *Nat. Mater.* **2024**, *23*, 1268.
- [15] J. Devkota, R. Geng, R. C. Subedi, T. D. Nguyen, *Adv. Funct. Mater.* **2016**, *26*, 3881.
- [16] C. Zhang, S. Ding, K. Qiao, J. Li, Z. Li, Z. Yin, J. Sun, J. Wang, T. Zhao, F. Hu, B. Shen, *ACS Appl. Mater. Interfaces* **2021**, *13*, 28442.
- [17] K. V. Raman, A. M. Kamerbeek, A. Mukherjee, N. Atodiressei, T. K. Sen, P. Lazić, V. Caciuc, R. Michel, D. Stalke, S. K. Mandal, S. Blügel, M. Münzenberg, J. S. Moodera, *Nature* **2013**, *493*, 509.
- [18] M. Cinchetti, V. A. Dediu, L. E. Hueso, *Nat. Mater.* **2017**, *16*, 507.
- [19] S. Steil, N. Großmann, M. Laux, A. Ruffing, D. Steil, M. Wiesenmayer, S. Mathias, O. L. A. Monti, M. Cinchetti, M. Aeschlimann, *Nat. Phys.* **2013**, *9*, 242.
- [20] S. Sanvito, *Nat. Phys.* **2010**, *6*, 562.
- [21] Z. H. Xiong, D. Wu, Z. V. Vardeny, J. Shi, *Nature* **2004**, *427*, 821.
- [22] J. Wang, C. Zhang, H. Liu, R. McLaughlin, Y. Zhai, S. R. Vardeny, X. Liu, S. McGill, D. Semenov, H. Guo, R. Tsuchikawa, V. V. Deshpande, D. Sun, Z. V. Vardeny, *Nat. Commun.* **2019**, *10*, 129.
- [23] S. Liang, H. Yang, H. Yang, B. Tao, A. Djeflal, M. Chshiev, W. Huang, X. Li, A. Ferri, R. Desfeux, S. Mangin, D. Lacour, M. Hehn, O. Copie, K. Dumesnil, Y. Lu, *Adv. Mater.* **2016**, *28*, 10204.
- [24] D. Sun, M. Fang, X. Xu, L. Jiang, H. Guo, Y. Wang, W. Yang, L. Yin, P. C. Snijders, T. Z. Ward, Z. Gai, X. G. Zhang, H. N. Lee, J. Shen, *Nat. Commun.* **2014**, *5*, 4396.
- [25] X. Sun, A. Bedoya-Pinto, Z. Mao, M. Gobbi, W. Yan, Y. Guo, A. Atxabal, R. Llopis, G. Yu, Y. Liu, A. Chuvilín, F. Casanova, L. E. Hueso, *Adv. Mater.* **2016**, *28*, 2609.
- [26] D. Sun, L. Yin, C. Sun, H. Guo, Z. Gai, X. G. Zhang, T. Z. Ward, Z. Cheng, J. Shen, *Phys. Rev. Lett.* **2010**, *104*, 236602.
- [27] S. Ding, Y. Tian, H. Wang, Z. Zhou, W. Mi, Z. Ni, Y. Zou, H. Dong, H. Gao, D. Zhu, W. Hu, *ACS Nano* **2018**, *12*, 12657.
- [28] L. Guo, X. Gu, S. Hu, W. Sun, R. Zhang, Y. Qin, K. Meng, X. Lu, Y. Liu, J. Wang, P. Ma, C. Zhang, A. Guo, T. Yang, X. Yang, G. Wang, Y. Liu, K. Wang, W. Mi, C. Zhang, L. Jiang, L. Liu, K. Zheng, W. Qin, W. Yan, X. Sun, *Nat. Commun.* **2024**, *15*, 865.
- [29] Z. Luo, Z. Yu, X. Lu, W. Niu, Y. Yu, Y. Yao, F. Tian, C. L. Tan, H. Sun, L. Gao, W. Qin, Y. Xu, Q. Zhao, X.-X. Song, *Nano Lett.* **2024**, *24*, 6183.
- [30] D. Ciudad, M. Gobbi, C. J. Kinane, M. Eich, J. S. Moodera, L. E. Hueso, *Adv. Mater.* **2014**, *26*, 7561.
- [31] T. D. Nguyen, G. Hukic-Markosian, F. Wang, L. Wojcik, X.-G. Li, E. Ehrenfreund, Z. V. Vardeny, *Nat. Mater.* **2010**, *9*, 345.
- [32] L. Schulz, L. Nuccio, M. Willis, P. Desai, P. Shakya, T. Kreouzis, V. K. Malik, C. Bernhard, F. L. Pratt, N. A. Morley, A. Suter, G. J. Nieuwenhuys, T. Prokscha, E. Morenzoni, W. P. Gillin, A. J. Drew, *Nat. Mater.* **2011**, *10*, 39.
- [33] S. Hu, W. Liu, L. Guo, R. Zhang, X. Gu, K. Meng, Y. Qin, A. Guo, T. Yang, C. Zhang, X. Yang, S. Lu, M. Wu, K. Lu, T. Tan, E. Zhou, Z. Wei, X. Sun, *Adv. Mater.* **2023**, *35*, 2300055.
- [34] X. Ding, J. Xue, S. Ding, C. Chen, X. Wang, X. Yu, W. Hu, *Angew. Chem., Int. Ed.* **2022**, *61*, 202208969.
- [35] T. D. Nguyen, E. Ehrenfreund, Z. V. Vardeny, *Science* **2012**, *337*, 204.
- [36] X. Sun, S. Vélez, A. Atxabal, A. Bedoya-Pinto, S. Parui, X. Zhu, R. Llopis, F. Casanova, L. E. Hueso, *Science* **2017**, *357*, 677.
- [37] J. P. Prieto-Ruiz, S. G. Miralles, H. Prima-García, A. López-Muñoz, A. Riminucci, P. Graziosi, M. Aeschlimann, M. Cinchetti, V. A. Dediu, E. Coronado, *Adv. Mater.* **2019**, *31*, 1806817.
- [38] M. Fang, Y. Wang, H. Wang, Y. Hou, E. Vetter, Y. Kou, W. Yang, L. Yin, Z. Xiao, Z. Li, L. Jiang, H. N. Lee, S. Zhang, R. Wu, X. Xu, D. Sun, J. Shen, *Nat. Commun.* **2020**, *11*, 2627.
- [39] D. Sun, E. Ehrenfreund, Z. V. Vardeny, *Chem. Commun.* **2014**, *50*, 1781.
- [40] W. Yang, Q. Shi, T. Miao, Q. Li, P. Cai, H. Liu, H. Lin, Y. Bai, Y. Zhu, Y. Yu, L. Deng, W. Wang, L. Yin, D. Sun, X. G. Zhang, J. Shen, *Nat. Commun.* **2019**, *10*, 3877.
- [41] C. Zhang, S. Ding, Y. Tian, J. Wang, Y. Chen, T. Zhao, F. Hu, W. Hu, B. Shen, *Small* **2023**, *19*, 2303375.
- [42] S. Hu, Y. Qin, S. Lu, L. Guo, X. Gu, T. Yang, R. Zhang, K. Meng, C. Zhang, M. Wu, X. Sun, *Adv. Funct. Mater.* **2024**, *34*, 2315239.
- [43] Y. Yang, M. M. Yang, Z. L. Luo, H. Huang, H. Wang, J. Bao, C. Hu, G. Pan, Y. Yao, Y. Liu, X. G. Li, S. Zhang, Y. G. Zhao, C. Gao, *Appl. Phys. Lett.* **2012**, *100*, 043506.
- [44] C. Song, B. Cui, F. Li, X. Zhou, F. Pan, *Prog. Mater. Sci.* **2017**, *87*, 33.
- [45] Y. Zhang, W. Sun, K. Cao, X.-X. Yang, Y. Yang, S. Lu, A. Du, C. Hu, C. Feng, Y. Wang, J. Cai, B. Cui, H.-G. Piao, W. Zhao, Y. Zhao, *Sci. Adv.* **2024**, *10*, ead14633.
- [46] W. Sun, Y. Zhang, K. Cao, S. Lu, A. Du, H. Huang, S. Zhang, C. Hu, C. Feng, W. Liang, Q. Liu, S. Mi, J. Cai, Y. Lu, W. Zhao, Y. Zhao, *Sci. Adv.* **2024**, *10*, eadj8379.
- [47] P. Li, A. Chen, D. Li, Y. Zhao, S. Zhang, L. Yang, Y. Liu, M. Zhu, H. Zhang, X. Han, *Adv. Mater.* **2014**, *26*, 4320.
- [48] H. S. Kum, H. Lee, S. Kim, S. Lindemann, W. Kong, K. Qiao, P. Chen, J. Irwin, J. H. Lee, S. Xie, S. Subramanian, J. Shim, S.-H. Bae, C. Choi, L. Ranno, S. Seo, S. Lee, J. Bauer, H. Li, K. Lee, J. A. Robinson, C. A. Ross, D. G. Schlom, M. S. Rzchowski, C.-B. Eom, J. Kim, *Nature* **2020**, *578*, 75.
- [49] A. Chen, Y. Wen, B. Fang, Y. Zhao, Q. Zhang, Y. Chang, P. Li, H. Wu, H. Huang, Y. Lu, Z. Zeng, J. Cai, X. Han, T. Wu, X.-X. Zhang, Y. Zhao, *Nat. Commun.* **2019**, *10*, 243.
- [50] H. Wang, Q. Zhao, Z. Ni, Q. Li, H. Liu, Y. Yang, L. Wang, Y. Ran, Y. Guo, W. Hu, Y. Liu, *Adv. Mater.* **2018**, *30*, 1803961.
- [51] M. Galbiati, S. Tatay, C. Barraud, A. V. Dediu, F. Petroff, R. Mattana, P. Seneor, *MRS Bull.* **2014**, *39*, 602.
- [52] A. J. Yang, K. Han, K. Huang, C. Ye, W. Wen, R. Zhu, R. Zhu, J. Xu, T. Yu, P. Gao, Q. Xiong, X. R. Wang, *Nat. Electron.* **2022**, *5*, 233.
- [53] J.-K. Huang, Y. Wan, J. Shi, J. Zhang, Z. Wang, W. Wang, N. Yang, Y. Liu, C.-H. Lin, X. Guan, L. Hu, Z.-L. Yang, B.-C. Huang, Y.-P. Chiu, J. Yang, V. Tung, D. Wang, K. Kalantar-Zadeh, T. Wu, X. Zu, L. Qiao, L.-J. Li, S. Li, *Nature* **2022**, *605*, 262.
- [54] G. Kresse, J. Furthmüller, *Phys. Rev. B* **1996**, *54*, 11169.
- [55] P. E. Blöchl, *Phys. Rev. B* **1994**, *50*, 17953.
- [56] J. P. Perdew, K. Burke, M. Ernzerhof, *Phys. Rev. Lett.* **1996**, *77*, 3865.
- [57] S. Grimme, S. Ehrlich, L. Goerigk, *J. Comput. Chem.* **2011**, *32*, 1456.
- [58] V. I. Anisimov, J. Zaanen, O. K. Andersen, *Phys. Rev. B* **1991**, *44*, 943.